liquids

MDPI

Article

Solvent Exchange around Aqueous Zn(II) from Ab Initio Molecular Dynamics Simulations

Adrian Malinowski and Maciej Śmiechowski *

Department of Physical Chemistry, Faculty of Chemistry, Gdańsk University of Technology, Narutowicza 11/12, 80-233 Gdańsk, Poland

* Correspondence: maciej.smiechowski@pg.edu.pl

Abstract: Hydrated zinc(II) cations, due to their importance in biological systems, are the subject of ongoing research concerning their hydration shell structure and dynamics. Here, ab initio molecular dynamics (AIMD) simulations are used to study solvent exchange events around aqueous Zn^{2+}, for which observation in detail is possible owing to the considerable length of the generated trajectory. While the hexacoordinated $Zn(H_2O)_6{}^{2+}$ is the dominant form of Zn(II) in an aqueous solution, there is a non-negligible contribution of the pentacoordinated $Zn(H_2O)_5{}^{2+}$ complex which presence is linked to the dissociative solvent exchange events around Zn^{2+}. The pentacoordinated Zn(II) has a much tighter hydration sphere and is characterized by a trigonal bipyramidal structure, in contrast to the usual octahedral symmetry of the hexacoordinated complex. In total, two full exchange events are registered in the analyzed trajectory. AIMD simulations on an adequate length scale thus provide a direct way of studying such solvent exchange events around ions in molecular detail.

Keywords: ab initio molecular dynamics; density functional theory; zinc(II) hydration; solvent exchange

Citation: Malinowski, A.; Śmiechowski, M. Solvent Exchange around Aqueous Zn(II) from Ab Initio Molecular Dynamics Simulations. *Liquids* **2022**, *2*, 243–257. https://doi.org/10.3390/liquids2030015

Academic Editor: Cory Pye

Received: 25 August 2022
Accepted: 14 September 2022
Published: 19 September 2022

1. Introduction

The coordination of zinc(II) cation is of paramount importance in biological systems, as zinc is the active center in hundreds of metalloenzymes, most often catalyzing hydrolysis reactions [1]. The importance of zinc goes beyond the role of cofactor in proteins, as the zinc cation is also actively utilized for intracellular signaling and subject to elaborate homeostasis mechanisms in the cell [2].

Due to the particular importance of water as the solvent in biological context, the structure and dynamics of hydrated ions is a topic of special significance in physical chemistry of solutions [3–5]. The influence of ions on water is often expressed in the terms of structural effects exerted by ions on the solvent, leading to the distinction between structure making and breaking ions [5].

The hydration of Zn(II) is also the subject of extensive research concerning its solvation shell structure and solvent exchange dynamics. To date, numerous experimental techniques have been applied to study Zn^{2+}(aq), including vibrational spectroscopy [6–12], extended X-ray absorption fine structure (EXAFS) [13–17], X-ray diffraction (XRD) [18–22], and neutron diffraction (ND) [23,24]. On the other hand, computational chemistry methods have also been used to obtain molecular-level data on zinc hydration. The static structure of aqueous complexes of Zn(II) has been comprehensively studied with quantum mechanical (QM) methods, using both wavefunction theory and density functional theory (DFT) [9,10,25–33]. Both structural and dynamical nature of the hydration phenomenona may be in turn investigated with molecular dynamics (MD) simulations with an increasing level of complexity. Zn(II) hydration has been studied with force field-based MD simulations [17,34–41], as well as quantum mechanics/molecular mechanics (QM/MM) MD simulations [42–46] and ab initio molecular dynamics (AIMD) simulations [47–50].

AIMD based on DFT is a particularly suited technique for studying aqueous ionic solutions [51,52]. Beginning with the pioneering study of Be^{2+}(aq) [53], many metal ions in an aqueous solution have been studied using AIMD simulations [54–58]. The current availability of fast and approximate DFT methods, such as density functional tight binding (DFTB) allows for the generation of extensive data sets on solvated ions in molecular solvents, including water [59]. The particular advantage of AIMD is the ability to study intermolecular polarization effects that ultimately influence many dynamic properties of the studied systems [54,55,60].

Computational methods are also indispensable for elucidating solvent exchange mechanisms around ions [61,62]. Experimental methods, rather than providing a mechanism of the exchange reaction, can only help in estimating the rate of this process [24]. The details of H_2O exchange around Zn(II) have been studied using MD simulations and static QM calculations [28–30,37]. Although AIMD simulations, combining the quantum description of electrons with the classical propagation of nuclei according to Newton's laws of motion, seem ideal for this purpose, the rather long timescale of water exchange in the first hydration shell of Zn(II) has thus far hampered direct observation of this process using AIMD.

In this work, in order to bridge this gap and obtain reliable data on the structure of Zn^{2+}(aq) and the dynamics of the solvent exchange process in its first hydration shell, we use extensive DFT-based AIMD simulations with a computational setup that is proven to be especially suitable for investigating liquid water. We hypothesize that the inability of hitherto equilibrium AIMD studies to register any solvent exchange around Zn(II) was a limitation of the short timescale of the simulations, rather than the flows in the method itself. We also aim to register the interplay of well-defined solvation complexes of Zn^{2+}(aq) that participate in the solvent exchange process.

2. Computational Methods

We studied aqueous Zn(II) in a system composed of a single Zn^{2+} cation and 100 H_2O molecules, which was contained in a cubic simulation supercell with applied periodic boundary conditions. The volume of the system was chosen to represent the experimental density of H_2O at 298 K (997 kg m^{-3} [63]) coupled with the absolute standard partial molar ionic volume of Zn^{2+}(aq) (-34.9 cm^3 mol^{-1} [64,65]), resulting in cell volume 14.33^3 $Å^3$. The starting configuration was prepared using GROMACS (v. 2018.5) tools [66] by solvating a centrally placed Zn^{2+} cation with a solvent configuration obtained from a well-equilibrated AMOEBA water simulation [67].

The system was initially subject to energy minimization and subsequently equilibrated using classical MD simulations in the canonical (NVT) ensemble at $T = 298.15$ K performed using Tinker-HP package (v. 1.2) [68]. The revised AMOEBA force field for liquid water [69] in combination with the AMOEBA parameterization of Zn(II) [38] were applied. The ultimate configuration from this NVT trajectory was then used to initialize the actual AIMD simulation.

AIMD simulations were performed with the cp2k computational suite (v. 6.0) [70–72], employing the DFT-based representation of the electronic structure as implemented in the Quickstep electronic structure module in cp2k [73]. The revPBE exchange-correlation functional [74,75] coded in the libXC library [76] was used, as it provides excellent reproduction of numerous static and dynamic properties of liquid water and aqueous ionic solutions [77–81]. A mixed Gaussian atomic orbitals with plane waves (GPW) representation of the electronic structure is applied in cp2k [82], and we used a molecularly optimized short-ranged double-zeta (DZVP-MOLOPT-SR-GTH) basis set for atomic orbitals [83], coupled with the auxiliary plane wave expansion of the electron density up to a 500 Ry cutoff. Though heavily contracted and featuring few diffuse primitive atomic orbitals, the chosen basis set performs favorably when compared to a more expensive triple-zeta polarized basis set for the description of liquid water [84]. Only valence electrons were treated explicitly, while core electrons were represented by norm-conserving GTH pseu-

dopotentials [85] parameterized for the PBE functional. Additionally, the smoothing of the electron density and its derivative on the spatial integration grid was applied (via keywords `XC_SMOOTH_RHO NN50` and `XC_DERIV NN50_SMOOTH` in cp2k), as it was previously found to significantly improve the stability of the local energetics of liquid water [86]. Dispersion effects were included via two-body DFT-D3 empirical dispersion correction with zero damping term [87] with the cutoff set to 15 Å. The studied system has a non-zero total charge (+2) and the charge compensation is provided by an implicit neutralizing jellium background [88], as implemented in cp2k.

The system was first equilibrated for ∼35 ps in an AIMD simulation in the canonical (NVT) ensemble at $T = 298.15$ K using the canonical velocity rescaling (CSVR) thermostat [89] with the time constant set to 2000 cm^{-1} (≈16.67 fs). The simulation time step was set to 0.5 fs. After this equilibration period, the thermostat was removed and a production AIMD simulation in the microcanonical (NVE) ensemble was continued for 100 ps, with data collection every 2 fs. The centers of maximally localized Wannier functions (MLWFs) [90] were also computed and stored every 2 fs. Analyses were performed using in-house code and VMD (v. 1.9.4) [91], which also served as a visualization tool, along with gnuplot (v. 5.2) [92].

3. Results

The static structure of the hydration shells of aqueous Zn(II) is summarized by radial distribution functions (RDFs) for the Zn···O and Zn···H pairs, as depicted in Figure 1. The studied system is large enough to fully contain two hydration shells of Zn^{2+}, as clearly seen in the Zn···O RDF that features a prominent shallow minimum with $g(r) \approx 0$ separating the first hydration shell from the second one. At first glance, the running integration number of $g_{ZnO}(r)$ is very close to 6 along this minimum, implying a predominantly hexacoordinated Zn(II) ion. However, its exact value of 5.8 suggests that during as much as 20% of the trajectory Zn^{2+} might in fact be pentacoordinated. Detailed parameters of the analyzed RDFs are gathered in Table 1.

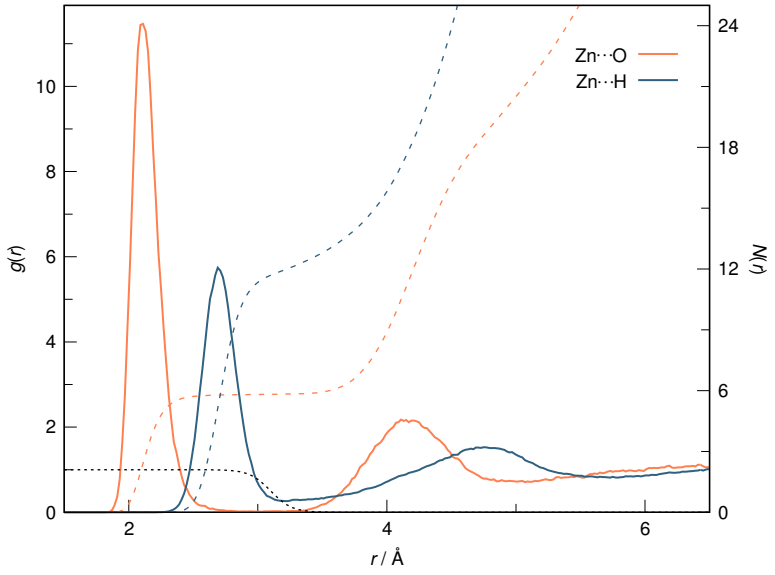

Figure 1. Radial distribution functions, $g(r)$, for Zn···O (orange) and Zn···H (blue) pairs (solid lines, left ordinate), as well as their running integrals, $N(r)$ (dashed lines, right ordinate). The black dotted line represents the smooth cutoff function used for water molecule coordination in Equation (1) (left ordinate).

Table 1. Most important parameters of the radial distribution functions depicted in Figure 1: location of the first and the second maxima and minima and the respective running integration numbers.

RDF	$r_{max,1}$ / Å	$r_{min,1}$ / Å	N_1 [1]	$r_{max,2}$ / Å	$r_{min,2}$ / Å	N_2 [2]
Zn···O	2.11	3.03	5.8	4.11	5.07	15.2
Zn···H	2.69	3.21	12.0	4.75	5.79	28.0

[1] $N_1 = N(r_{min,1})$; [2] $N_2 = N(r_{min,2}) - N(r_{min,1})$.

The first hydration shell of Zn^{2+} extends up to 3.03 Å and contains a non-integer number of water oxygen atoms. In order to determine the instantaneous coordination number (CN) of Zn(II), one could simply count O atoms found closer than the $r_{min,1}$ value, which would be tantamount to accepting the Heaviside step function as a selector function for H_2O molecules. However, this results in a discontinuous CN trajectory and adopting a smooth selector function instead can help visualize transitions between different coordination states of Zn^{2+}(aq), as previously proposed [50]. In this work, the coordinated solvent molecules are selected using a logistic cutoff function:

$$CN(t) = \sum_{i=1}^{N_{H_2O}} \frac{1}{1 + e^{\frac{r_{ZnO,i}(t) - r_0}{s}}}, \quad (1)$$

controlled by the cutoff radius r_0 and the sharpness parameter s. $r_{ZnO,i}(t)$ is the instantaneous Zn···O distance for the water molecule i. Adopting $r_0 = 3.1$ Å and $s = 0.08$ Å ensures a smooth transition between a fully coordinated H_2O molecule in the first hydration shell, where $CN_i(t) \to 1$, and a non-coordinated molecule in the second hydration shell, where $CN_i(t) \to 0$, cf. Figure 1.

The time evolution of thus obtained smooth coordination number of Zn^{2+} is shown in Figure 2. As clearly seen, even though a continuous $CN(t)$ definition is accepted, its value provides a clear-cut distinction between the hexa- and pentacoordinated states of aqueous Zn(II). The zinc cation spends most of the time in a $Zn(H_2O)_6^{2+}$ complex (about 81.2% of the trajectory). The pentacoordinated complex may be unanimously found in ∼16.3% of the trajectory, while we ascribe the rest to transitional structures or short-time existence periods of one of the two dominating structures that are too short for inclusion in the analysis.

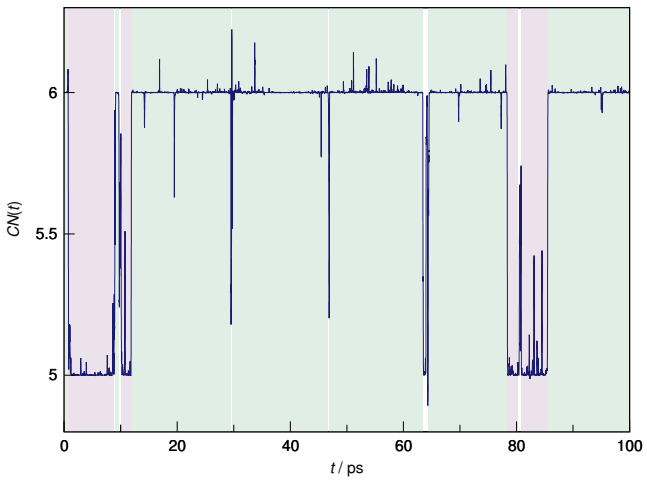

Figure 2. Time evolution of the smooth coordination number of Zn^{2+}, $CN(t)$, along the AIMD production trajectory. Light green and light purple areas indicate regions assigned to hexa- and pentacoordinated aqueous Zn(II) complexes, respectively, while white regions indicate transitional periods excluded from detailed analysis.

Armed with the knowledge about the existence of two distinct coordination states of Zn^{2+}(aq), we revisit Figure 1 in order to compare the Zn···O RDFs in the regions of existence of the hexa- and pentacoordinated complexes. As seen in Figure 3, there is only a slight difference between the RDF based on the entire trajectory and the one based only on the fragments where $Zn(H_2O)_6^{2+}$ is found, which is unsurprising given the predominance of the hexacoordinated Zn(II). More importantly, the Zn···O RDF restricted to the trajectory periods where $Zn(H_2O)_5^{2+}$ exists reveals a major compression of not only the first but also the second hydration shell of the zinc cation. The first maximum shifts to 2.07 Å, while the second one to 4.07 Å. Thus, the two distinct complexes are characterized with different hydration patterns extending up to the entire second hydration shell.

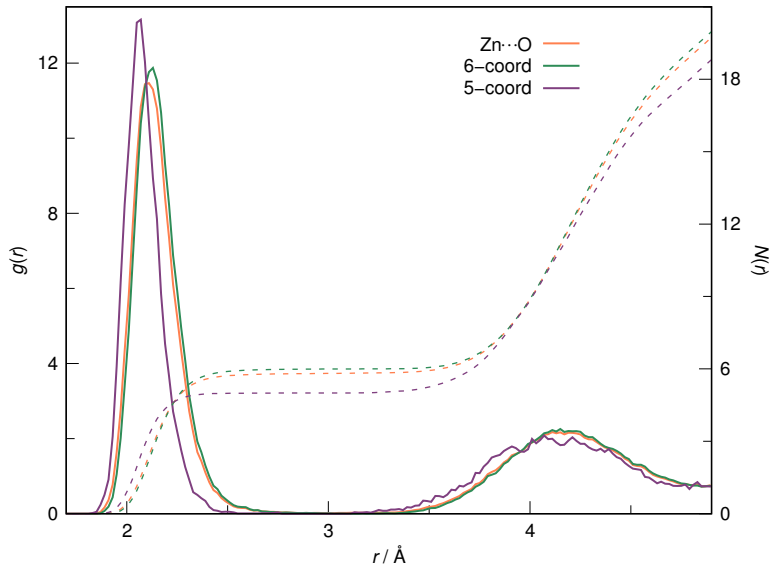

Figure 3. Radial distribution functions, $g(r)$, for Zn···O pairs averaged over the entire AIMD trajectory (orange), as well as only over the regions of existence of hexacoordinated (green) and pentacoordinated (purple) aqueous Zn(II) complexes (solid lines, left ordinate), together with their running integrals, $N(r)$ (dashed lines, right ordinate).

Unlike static geometry optimizations, AIMD simulations can provide ensemble-averaged structures. In order to find the preferred geometry of hexa- and pentacoordinated Zn^{2+}(aq), we isolated the first shell complexes from the relevant trajectory fragments, rotated them to a common reference frame and averaged the geometry. The results can be seen in Figure 4. $Zn(H_2O)_6^{2+}$ forms a regular octahedral complex with the average Zn···O distance equal 2.14 Å. On the contrary, $Zn(H_2O)_5^{2+}$ is characterized by a trigonal bipyramidal arrangement of water ligands. The Zn···O distance for the three equatorial molecules is 2.04 Å, while the axial O atoms are located on average 2.14 Å from the metal cation. The geometries of the two complexes in Cartesian coordinates are available in the Supplementary Materials, see Figure S1.

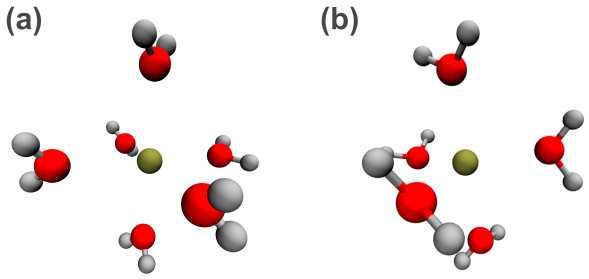

Figure 4. Time-averaged structure of (**a**) $Zn(H_2O)_6^{2+}$ and (**b**) $Zn(H_2O)_5^{2+}$ extracted from the respective regions of the AIMD trajectory.

While the positions of O atoms tend to be fixed in the Zn(II) solvation cage, the hydrogen atoms of the first shell water molecules are relatively free to bend from the coplanar arrangement with the Zn–O vector. We define the tilt angle, β, as the angle formed between the Zn–O vector and the dipole moment vector of the coordinated H_2O molecule. The two-dimensional distribution of water molecule configurations in the (r_{ZnO}, β) plane is shown in Figure 5. The distribution of angles is evidently bimodal, with a global maximum at 0°, indicating a coplanar arrangement of the H_2O molecular plane and the Zn–O vector, and a local maximum at ca. 30°, reflecting the presence of a substantial population of water molecules with tilted H atoms. We note here that the latter tend to be located slightly farther away from the central atom.

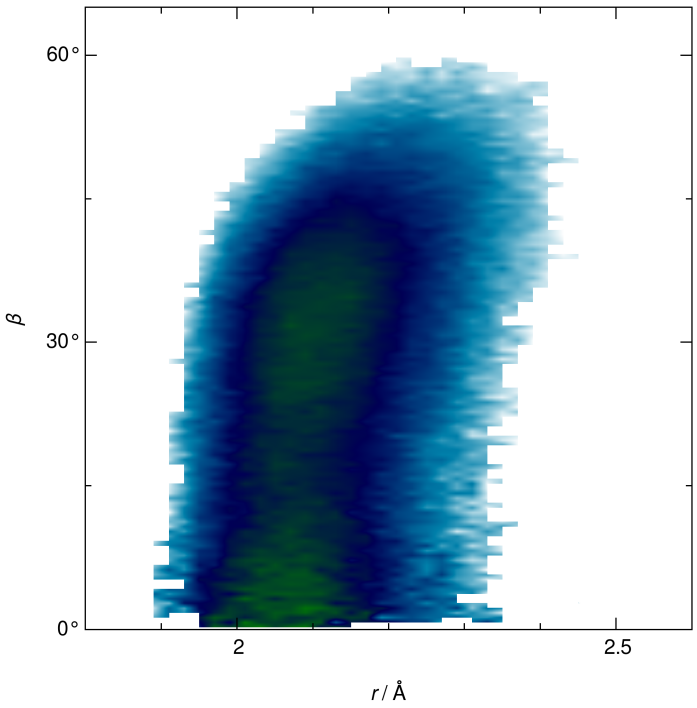

Figure 5. The two-dimensional distribution function, $g(r_{ZnO}, \beta)$, drawn on a logarithmic scale as $-\log g(r_{ZnO}, \beta)$ where β is the tilt angle of the coordinated H_2O molecule as defined in the text.

The presence of two complexes in aqueous solution of Zn(II) has far-reaching implications for the water molecules in its hydration shell. Ions are known to polarize water and the extent of this polarization is related to the changes in infrared spectrum of solution with respect to bulk water [54,55]. In Figure 6 we compare the probability distribution functions of the length of molecular dipoles of H_2O molecules in the entire system vs the ones in the first hydration shell of Zn^{2+}(aq). Unlike the dipole moment in bulk water, which has a symmetric Gaussian distribution [54,55,60], the curve for the studied system

is right-skewed due to the substantial polarization of the neighboring H_2O molecules by the zinc cation. The distribution can be fitted to a split Pearson VII peak shape with a maximum located at 2.78 D. On the contrary, the distributions of dipole moments of water molecules found in the two complexes are symmetric and can similarly be fit to a Pearson VII analytical shape. It is found that H_2O molecules in $Zn(H_2O)_5^{2+}$ are polarized more significantly (on average 3.71 D) than the ones in $Zn(H_2O)_6^{2+}$ (mean 3.43 D).

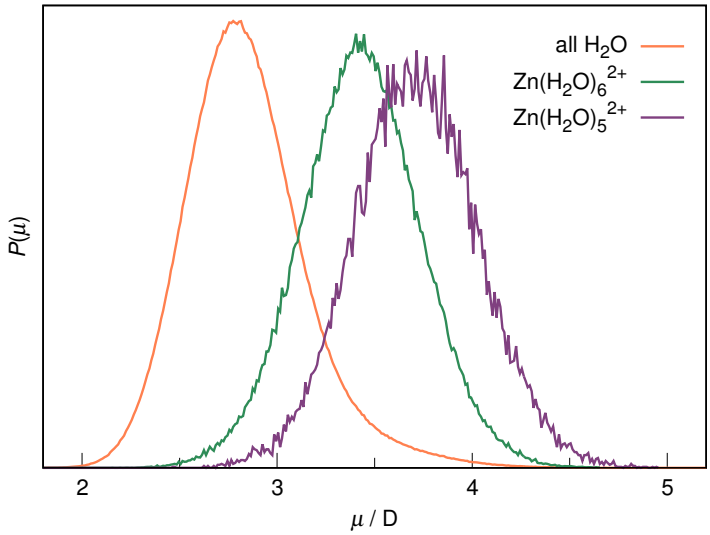

Figure 6. Normalized distribution functions of the molecular dipole moments of water molecules in the studied system, as well as water molecules in $Zn(H_2O)_6^{2+}$ (green) and $Zn(H_2O)_5^{2+}$ (purple).

We finally would like to estimate the time frame of a single exchange event based on the trajectories of the participating water molecules. As seen in Figure 2, we register two major exchange events connected to a change in CN of Zn(II), at around 0–12 ps and again at 78–86 ps. Additionally, a short-lived occurrence of $Zn(H_2O)_5^{2+}$ is found at ca. 64 ps. In order to shed light on the molecular details of these exchange events, we plotted the time evolution of the Zn$\cdots$O distance of involved H_2O molecules, as presented in Figure 7.

The first event begins as soon as the production trajectory starts. The water molecule W_{47} dissociates from the initially present $Zn(H_2O)_6^{2+}$ at 0.72–0.75 ps. Hereafter, the W_n notation indicates a H_2O molecule with an arbitrary index n in the trajectory. The solvent exchange process is obviously dissociative, as no new solvent molecule coordinates to the cation for an extended period of time. In this event, the released H_2O moves to the second hydration shell, as its separation from Zn^{2+} increases to ca. 4 Å (cf. Figure 1). This results in a transient $Zn(H_2O)_5^{2+}$ complex that persists up to ~8.8 ps, at which moment an interesting concerted mechanism is observed. Namely, W_{47} is kicked off to the weakly organized third hydration shell of the cation, at 6 Å and beyond, while another second shell H_2O, specifically W_{12}, coordinates to zinc(II), restoring the $Zn(H_2O)_6^{2+}$ complex. This, however, proves short-lived, as W_{12} dissociates already at ~10.1 ps and returns to the second hydration shell. Since a similar phenomenon is observed in further events, *vide infra*, such attempted exchange events that ultimately fail to stabilize the newly formed complex are most probably a common occurrence in Zn^{2+}(aq). Somewhat surprisingly, the entire exchange event is finalized by a third water molecule (W_{22}) that is captured by Zn^{2+} not from the second, but rather directly from the third hydration shell, initially >6 Å away from the cation. The hexacoordinated complex is restored at ~11.9 ps and remains stable for an extended period of time. Interestingly, the coordination of W_{22} is seemingly again assisted by W_{47}, since the time of arrival of the latter in the third hydration shell coincides with the start of movement of the former towards the inner hydration shells.

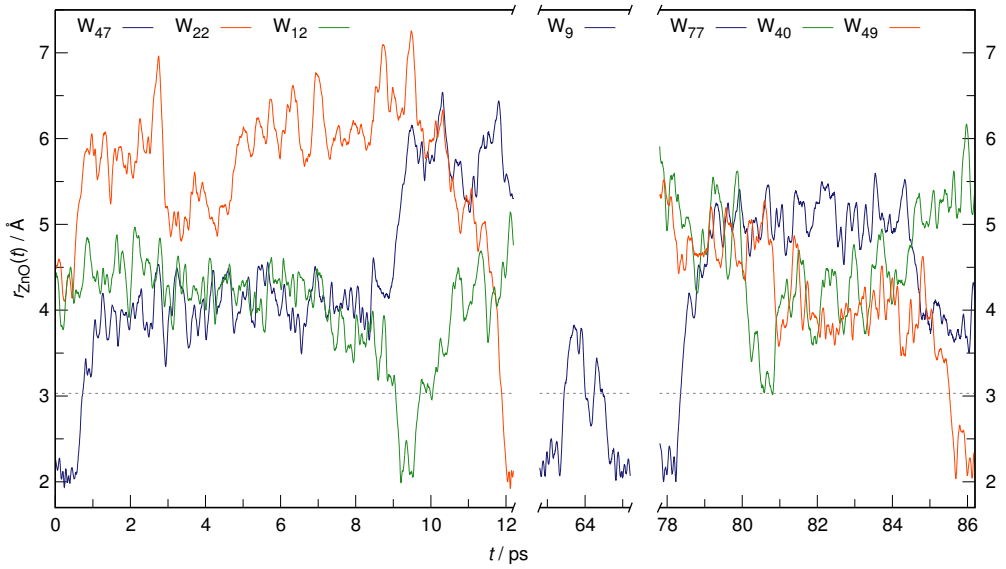

Figure 7. Major successful and attempted exchange events registered during the AIMD production trajectory as depicted by the Zn···O distance of the participating water molecules. The W_n labels refer to the arbitrary index of the H_2O molecule in the trajectory. Line colors indicate the leaving molecule (blue), the incoming molecule (red), as well as the intervening molecule (green). Black dotted line shows the location of the first minimum in the Zn···O radial distribution function (3.03 Å). Note the discontinuous abscissa axis.

The second exchange event is only an attempted escape of W_9 from $Zn(H_2O)_6^{2+}$ at ca. 64 ps. However, no other H_2O molecule tries to enter the first hydration shell of Zn(II) this time and ultimately, after transiently wandering off to the verge of the second shell, W_9 is recaptured by the complex and the stable octahedral arrangement of ligands persists.

The third exchange event (and the second successful one) resembles the first one to a great extent. It begins with the dissociation of W_{77} at ca. 78.3 ps. This H_2O molecule is released initially to the second hydration shell, but quickly travels further to ultimately stay at ca. 5 Å separation from zinc(II) for an extended period, which is the location of the shallow minimum between the second and the poorly defined third hydration shell of the cation (cf. Figure 1). Interestingly, this perturbation of the hydration shells leads to two concerted movements of water molecules towards the central complex, initially that of W_{40}, quickly followed by W_{49}. Similarly to the first exchange event, the intervening water molecule (here, W_{40}) ultimately does not manage to become properly coordinated to the cation. Instead, it remains at the very edge of the first hydration shell, only sligthly perturbing the newly formed $Zn(H_2O)_5^{2+}$ complex. After its release back into the second hydration shell at ca. 81 ps, the pentacoordinated complex remains stable for almost 4 ps. Then, an interesting cascade of concerted events can be noticed. W_{77} returns to the second hydration shell, apparently swapping its place with W_{40}, but at the same time W_{49} manages to get captured by zinc(II), reinstating the hexacoordinated complex. Again, concerted movement of H_2O molecules seems to be crucial for the mutually assisted exchanges between solvation shells leading to coordination number change of Zn^{2+}(aq).

4. Discussion

The coordination of Zn^{2+}(aq) has been hitherto the subject of numerous experimental and computational studies, as reviewed in the Introduction. There is an overwhelming consensus that Zn(II) forms a hexahydrated complex with the structure of a regular octahedron (point group O_h for the ZnO_6 core) [9–11,14–21,25,27,32,34–36,38,40–48,50,93]. Reports claiming predominantly pentacoordinated Zn^{2+}(aq) do surface [28,29,31,33,49,94], but appear to suffer from a size effect, i.e., the undercoordination of Zn(II) occurs most commonly in small aqueous clusters and the $Zn(H_2O)_6^{2+}$ complex is uniformly restored

in the bulk limit [32,40]. Most notably for the present study, the coordination number of Zn(II) in an aqueous solution found from AIMD simulations seems to be dependent on the computational protocol, with dispersion corrections deemed particularly necessary to stabilize the $Zn(H_2O)_6^{2+}$ complex [50].

The Zn···O distances found experimentally and in computational investigations have been compiled by several authors [3,9,15,23,42,46,48,95]. EXAFS measurements find $r_{ZnO} = 2.05–2.13$ Å [13–17], while a survey of reported XRD investigations leads to a possible range of $r_{ZnO} = 2.08–2.17$ Å [3,18–22]. The available AIMD simulations report also a considerable spread of $r_{ZnO} = 2.02–2.18$ Å [47–50] while a slightly narrower range ($r_{ZnO} = 2.11–2.16$ Å) is reported from QM/MM MD simulations [42–46]. In comparison, our global average of the position of the first peak in $g_{ZnO}(r)$ (2.11 Å, see Figure 1 and Table 1) is generally in the middle of the reported distances.

The particular advantage of our analysis is the rigorous separation of the trajectory fragments with hexa- vs. pentacoordinated Zn(II), thanks to the smooth instantaneous coordination number, see Figure 2. This allowed us to prove the tightening of the hydration shells of Zn^{2+}(aq) with the dissociation of one H_2O from the complex. Our results for the most probable Zn···O distance in $Zn(H_2O)_6^{2+}$ vs $Zn(H_2O)_5^{2+}$ (2.13 Å and 2.07 Å, respectively, cf. Figure 3) are in good agreement with earlier AIMD simulations, a similar separation of trajectory fragments was proposed (2.11 Å and 2.05 Å, respectively [50]). Static geometry optimizations also lead to a general conclusion that the water molecules are located closer to Zn(II) in $Zn(H_2O)_5^{2+}$ than in $Zn(H_2O)_6^{2+}$ [26,27,29,31,32]. The hexacoordinated complex always maintains the octahedral arrangement of water oxygens (although the inclusion of hydrogens lowers the point group to T_h [9]), which is also found in our time-averaged structure, cf. Figure 4. More controversial is the preferred geometry of $Zn(H_2O)_5^{2+}$. Based on geometry optimizations, both trigonal bipyramid (point group D_{3h}) [26,31,32] and square pyramid (point group C_{2v}) [27,29,94] have been confirmed as minima of the potential energy surface. It appears though that the presence of second shell H_2O molecules stabilizes the former structure [29,40,94]. The presence of external hydration shells is thus crucial to the observation of the time-averaged trigonal bipyramidal structure that we report here, see Figure 4. The discrepancy between the Zn···O distance to equatorial and axial molecules (2.04 Å and 2.14 Å, respectively) is similar to that found previously in an isolated cluster (2.05 Å and 2.13 Å, respectively [26]).

Notably for AIMD simulations, our considerable system size with 100 H_2O molecules allows us to record the RDF for the entire second hydration shell, as well as for the weakly formed third shell, see Figure 1. Due to the structure-making nature of Zn^{2+}(aq), the second shell is also accessible experimentally. Previous EXAFS results indicate a second shell of 12.2 O atoms at an average distance of 4.40 Å [16] or 11.2 O atoms at 4.10 Å [14]. The distance to second shell from XRD measurements equals 4.02–4.26 Å [20–22]. Results from AIMD and QM/MM MD simulations generally support these experimental findings, with second hydration shell composed of 13–15 molecules at an average distance 4.3–4.5 Å [42,43,48,50]. In comparison, our global average of the position of the second peak in $g_{ZnO}(r)$ (4.11 Å, see Figure 1 and Table 1) is generally in the lower limit of the reported distances, while the number of O atoms (15.2) indicates a fairly crowded second hydration shell of Zn(II). Most importantly, the lowering of CN of the cation results in a major compression of this shell, with the RDF peak shifted to 4.07 Å (see Figure 3) and at least two water molecules released to the bulk solution, as the number of O atoms in the second shell decreases to 13.

Earlier studies on monovalent ions found that they are strongly polarized by water, but in turn do not polarize the solvent significantly (in the sense of only slight alteration of H_2O dipole moment) [54,55,60]. In strike contrast to these findings, the water molecules in the first hydration shell of Zn^{2+}(aq) are heavily polarized by the electric field of the cation, see Figure 6. For all H_2O molecules, we find an average dipole moment of 2.78 D, which is slightly lower than the value usually found in AIMD simulations of liquid water (∼3 D) [54,60]. However, mean dipole moment of liquid H_2O for revPBE/revPBE0 functionals is indeed slightly lower and in agreement with the present findings [96,97]. While the

increase of dipole moment of H_2O near the cation was previously found in MD simulations with the polarizable Amoeba force field, as well as AIMD simulations [38,48], the clear advantage of our analysis is the ability to separate the two forms of hydrated Zn(II). In the hexacoordinated complex, the dipole moment of the first shell water molecules increases by 0.65 D with respect to the bulk. Dissociation of this complex leads to a further increase of the average dipole moment and it is almost 1 D greater than for non-coordinated H_2O. Thus, the water molecules in $Zn(H_2O)_5^{2+}$ are evidently more heavily polarized than in $Zn(H_2O)_6^{2+}$. The 0.6 D increase of the mean dipole moment of first hydration shell H_2O has been noted previously in AIMD simulations [48]. Simulations with the Amoeba force field indicate that the water molecules closest to the cation have their dipole moments raised by more than 1 D [38].

Computational methods are excellent tools for studying solvent exchange mechanism around solvated ions [62]. The experimental estimate of water residence time on Zn(II) from quasi-elastic neutron scattering is a rather broad range of 0.1–5 ns [24]. Assuming the actual residence time is near the lower limit, it is in principle accessible to longer MD simulations. Previously, only force field description of the potential energy surface could provide the possibilities to reach the required time scale. However, the exact formulation of Zn(II)–H_2O interactions is crucial for enabling solvent exchange events and they were frequently not observed even in prolonged MD simulations [16,34–36]. On the other hand, a water residence time of 2.2 ns was found in an MD simulation with the Amoeba force field [38] and a rate constant for water exchange equal 4.1×10^8 s^{-1} was also obtained [37]. Most AIMD or QM/MM MD simulations to date suffered from length limitations and no exchange events were observed [42–48]. In stark contrast to these earlier results, we managed to register two full solvent exchange events in the first hydration shell of Zn(II). While it is impossible to quantitatively estimate the water residence time from such a small sample, we note that the starts of successful exchange events are separated by ca. 78 ps, so that our results are not in disagreement with the experimental estimates provided the true residence time is close to the lower limit proposed previously [24]. We note here that the solvent exchange may be studied using accelerated sampling, e.g., metadynamics [37,50,93]; however, while such an approach provides the details of the potential energy surface of the hydrated cation, only equilibrium simulations can capture the actual timescale of the observed events.

Unfortunately, the question of how the two complexes differ on the free energy scale cannot be answered directly from our equilibrium simulation. However, we can roughly estimate this free energy difference from the fractions of the trajectory attributed to the penta- and hexacoordinated structures as $\Delta G = -RT \ln(0.163/0.812) \approx 4$ kJ mol^{-1}. On the one hand, this is high enough that the pentacoordinated structure might prove too elusive to be registered experimentally, e.g., with EXAFS, noting also that the average coordination number of Zn(II) (5.8) is within the typical uncertainty of structure determination methods from the value of 6.0, indicative of perfect hexacoordination. On the other hand, this is low enough (only $1.6RT$) to allow relatively free interconversion between the two structures. We note here that the free energy difference between $[UO_2(H_2O)_5]^{2+}$(aq) and $[UO_2(H_2O)_4]^{2+}$(aq) from ab initio metadynamics is ~3 kJ mol^{-1}, with similarly inconclusive experimental results as in the case of Zn(II) [98].

Our results indicate that the solvent exchange around Zn(II) follows a dissociative mechanism, cf. Figure 7. The release of a single water molecule from the first hydration shell leads to a transient $Zn(H_2O)_5^{2+}$ complex, the lifetime of which may be tentatively estimated as 8–10 ps, based on the limited sample of events we registered. A similar timescale of dissociative exchange events was noted before by Fatmi et al. [43]. A similar mechanism of solvent exchange around hexacoordinated Zn(II) was also inferred from static QM calculations [29,30,62]. Interestingly, the dissociation of a water molecule does not lead to increased CN in the second shell. On the contrary, it undergoes compression and major structural changes, as evident from Figure 3. Consequently, the registered exchange events require concerted movement of assisting solvent molecules, cf. Figure 7.

This cooperative movement of H_2O molecules enables the capture of a newly coordinated water molecule from as far as the third solvation shell of Zn(II).

5. Conclusions

In this paper, the structure of the hydrated zinc(II) cation has been studied using extensive AIMD simulations. In contrast to numerous earlier MD investigations at different levels of theory, which frequently found only hexacoordinated zinc with fixed first hydration shell waters, we clearly identify the presence of both hexa- and pentacoordinated complexes of Zn^{2+}. While the octahedral $Zn(H_2O)_6{}^{2+}$ remains the dominant form of Zn(II) in an aqueous solution, $Zn(H_2O)_5{}^{2+}$ is present in about 16% of the trajectory. The average structure of the latter is a trigonal bipyramid and its presence results in major structural changes reaching up to the second hydration shell and beyond. Radial distribution functions indicate major compression of the second hydration shell of the pentacoordinated complex and molecular dipole distributions show profound polarization of first shell H_2O molecules that is also heavily dependent on CN.

Owing to the considerable length of the generated trajectory, we were able to register two full solvent exchange events around aqueous Zn^{2+}. They undoubtedly follow a dissociative mechanism and are driven by concerted solvent movement that may feature molecules up to the third hydration shell of Zn(II). While, due to the limited sampling, we cannot quantitatively estimate the water residence time on the zinc cation, the separation of successful events by ca. 80 ps seems to be consistent with the lower limit of experimental residence times (about 0.1 ns). The single exchange event, accompanied by the presence of $Zn(H_2O)_5{}^{2+}$, seems to take about 8–10 ps.

We conclude that equilibrium AIMD simulations on an adequate length scale provide a direct way of studying solvent exchange events around aqueous ions in molecular detail. The smooth selector function for coordinated solvent is a powerful tool that allows the identification of solvent exchange events and their preferred (associative or dissociative) mechanism. The analysis framework presented here may be tremendously useful for other solvated ions and more complicated systems containing Zn(II), such as concentrated zinc halide solutions.

Supplementary Materials: The following supporting information can be downloaded at: https://www.mdpi.com/article/10.3390/liquids2030015/s1, Figure S1: Cartesian coordinates of the structures from Figure 4.

Author Contributions: Conceptualization, methodology, supervision, writing—original draft preparation, M.Ś.; investigation, formal analysis, visualization, writing—review and editing, A.M. and M.Ś. All authors have read and agreed to the published version of the manuscript.

Funding: This research received no external funding.

Data Availability Statement: The data presented in this study are available on request from the corresponding author.

Acknowledgments: Calculations were performed at the Academic Computer Center in Gdańsk (TASK).

Conflicts of Interest: The authors declare no conflict of interest.

Abbreviations

The following abbreviations are used in this manuscript:

AIMD	ab initio molecular dynamics
CN	coordination number
DFT	density functional theory
DFTB	density functional tight binding
EXAFS	extended X-ray absorption fine structure

GTH	Goedecker–Teter–Hutter (pseudopotentials)
MD	molecular dynamics
MLWF	maximally localized Wannier function
ND	neutron diffraction
QM	quantum mechanics
QM/MM	quantum mechanics/molecular mechanics
revPBE	revised Perdew–Burke–Ernzerhof (functional)
XRD	X-ray diffraction

References

1. Coleman, J.E. Zinc enzymes. *Curr. Opin. Chem. Biol.* **1998**, *2*, 222–234. [CrossRef]
2. Maret, W. Zinc Biochemistry: From a Single Zinc Enzyme to a Key Element of Life. *Adv. Nutr.* **2013**, *4*, 82–91. [CrossRef]
3. Ohtaki, H.; Radnai, T. Structure and Dynamics of Hydrated Ions. *Chem. Rev.* **1993**, *93*, 1157–1204. [CrossRef]
4. Bakker, H.J. Structural Dynamics of Aqueous Salt Solutions. *Chem. Rev.* **2008**, *108*, 1456–1473. [CrossRef]
5. Marcus, Y. Effect of Ions on the Structure of Water: Structure Making and Breaking. *Chem. Rev.* **2009**, *109*, 1346–1370. [CrossRef]
6. Kristiansson, O.; Eriksson, A.; Lindgren, J. Hydration of Ions in Aqueous Solutions Studied by Infrared Spectroscopy. II. Application. *Acta Chem. Scand. A* **1984**, *38*, 613–618. [CrossRef]
7. Stangret, J.; Libuś, Z. Influence of Zn(II), Mn(II), and Mg(II) Cations on the Vibrational Spectra of Water in Aqueous Perchlorate Solutions. *Spectrosc. Lett.* **1988**, *21*, 397–412. [CrossRef]
8. Å. Bergström, P.; Lindgren, J.; Sandström, M.; Zhou, Y. Infrared Spectroscopic Study on the Hydration of Mercury(II), Cadmium(II), and Zinc(II) in Aqueous Solution and in the Hexahydrated Perchlorate Salts. *Inorg. Chem.* **1992**, *31*, 150–152. [CrossRef]
9. Rudolph, W.W.; Pye, C.C. Zinc(II) hydration in aqueous solution. A Raman spectroscopic investigation and an ab-initio molecular orbital study. *Phys. Chem. Chem. Phys.* **1999**, *1*, 4583–4593. [CrossRef]
10. Rudolph, W.W.; Pye, C.C. Zinc(II) Hydration in Aqueous Solution: A Raman Spectroscopic Investigation and An ab initio Molecular Orbital Study of Zinc(II) Water Clusters. *J. Solut. Chem.* **1999**, *28*, 1045–1070. [CrossRef]
11. Mink, J.; Németh, C.; Hajba, L.; Sandström, M.; Goggin, P.L. Infrared and Raman spectroscopic and theoretical studies of hexaaqua metal ions in aqueous solution. *J. Mol. Struct.* **2003**, *661–662*, 141–151. [CrossRef]
12. Wei, Z.F.; Zhang, Y.H.; Zhao, L.J.; Liu, J.H.; Li, X.H. Observation of the First Hydration Layer of Isolated Cations and Anions through the FTIR-ATR Difference Spectra. *J. Phys. Chem. A* **2005**, *109*, 1337–1342. [CrossRef]
13. Miyanaga, T.; Watanabe, I.; Ikeda, S. Amplitude in EXAFS and Ligand Exchange Reaction of Hydrated 3d Transition Metal Complexes. *Chem. Lett.* **1988**, *17*, 1073–1076. [CrossRef]
14. noz Páez, A.M.; Pappalardo, R.R.; Marcos, E.S. Determination of the Second Hydration Shell of Cr^{3+} and Zn^{2+} in Aqueous Solutions by Extended X-ray Absorption Fine Structure. *J. Am. Chem. Soc.* **1995**, *117*, 11710–11720. [CrossRef]
15. Kuzmin, A.; Obst, S.; Purans, J. X-ray absorption spectroscopy and molecular dynamics studies of Zn^{2+} hydration in aqueous solutions. *J. Phys. Condens. Matter* **1997**, *9*, 10065–10078. [CrossRef]
16. D'Angelo, P.; Barone, V.; Chillemi, G.; Sanna, N.; Meyer-Klaucke, W.; Pavel, N.V. Hydrogen and Higher Shell Contributions in Zn^{2+}, Ni^{2+}, and Co^{2+} Aqueous Solutions: An X-ray Absorption Fine Structure and Molecular Dynamics Study. *J. Am. Chem. Soc.* **2002**, *124*, 1959–1967. [CrossRef]
17. Migliorati, V.; Mancini, G.; Tatoli, S.; Zitolo, A.; Filipponi, A.; De Panfilis, S.; Di Cicco, A.; D'Angelo, P. Hydration Properties of the Zn^{2+} Ion in Water at High Pressure. *Inorg. Chem.* **2013**, *52*, 1141–1150. [CrossRef]
18. Bol, W.; Gerrits, G.J.A.; Van Panthaleon Van Eck, C.L. The Hydration of Divalent Cations in Aqueous Solution. An X-ray Investigation with Isomorphous Replacement. *J. Appl. Cryst.* **1970**, *3*, 486–492. [CrossRef]
19. Ohtaki, H.; Yamaguchi, T.; Maeda, M. X-Ray Diffraction Studies of the Structures of Hydrated Divalent Transition-Metal Ions in Aqueous Solution. *Bull. Chem. Soc. Jpn.* **1976**, *49*, 701–708. [CrossRef]
20. Licheri, G.; Paschina, G.; Piccaluga, G.; Pinna, G. X-ray Diffraction Study of Aqueous Solutions of $ZnSO_4$. *Z. Naturforsch.* **1982**, *37*, 1205–1210. [CrossRef]
21. Radnai, T.; Palinkas, G.; Caminiti, R. X-Ray Diffraction Study on Hydration and Ion-Pairing in Aqueous $ZnSO_4$ Solution. *Z. Naturforsch.* **1982**, *37*, 1247–1252. [CrossRef]
22. Dagnall, S.P.; Hague, D.N.; Towl, A.D.C. X-ray Diffraction Study of Aqueous Zinc(II) Nitrate. *J. Chem. Soc. Faraday Trans. 2 Mol. Chem. Phys.* **1982**, *78*, 2161–2167. [CrossRef]
23. Powell, D.H.; Gullidge, P.M.N.; Neilson, G.W.; Bellissent-Funel, M.C. Zn^{2+} hydration and complexation in aqueous electrolyte solutions. *Mol. Phys.* **1990**, *71*, 1107–1116. [CrossRef]
24. Salmon, P.S.; Bellissent-Funel, M.C.; Herdman, G.J. The dynamics of aqueous Zn^{2+} solutions: A study using incoherent quasi-elastic neutron scattering. *J. Phys. Condens. Matter* **1990**, *2*, 4297–4309. [CrossRef]
25. Mhin, B.J.; Lee, S.; Cho, S.J.; Lee, K.; Kim, K.S. $Zn(H_2O)_6^{2+}$ is very stable among aqua-Zn(II) ions. *Chem. Phys. Lett.* **1992**, *197*, 77–80. [CrossRef]
26. Bock, C.W.; Katz, A.K.; Glusker, J.P. Hydration of Zinc Ions: A Comparison with Magnesium and Beryllium Ions. *J. Am. Chem. Soc.* **1995**, *117*, 3754–3765. [CrossRef]

27. Lee, S.; Kim, J.; Park, J.K.; Kim, K.S. Ab Initio Study of the Structures, Energetics, and Spectra of Aquazinc(II). *J. Phys. Chem.* **1996**, *100*, 14329–14338. [CrossRef]
28. Hartmann, M.; Clark, T.; van Eldik, R. Theoretical Study of the Water Exchange Reaction on Divalent Zinc Ion using Density Functional Theory. *J. Mol. Model.* **1996**, *2*, 354–357. [CrossRef]
29. Hartmann, M.; Clark, T.; van Eldik, R. Hydration and Water Exchange of Zinc(II) Ions. Application of Density Functional Theory. *J. Am. Chem. Soc.* **1997**, *119*, 7843–7850. [CrossRef]
30. Rotzinger, F.P. Mechanism of Water Exchange for the Di- and Trivalent Metal Hexaaqua Ions of the First Transition Series. *J. Am. Chem. Soc.* **1997**, *119*, 5230–5238. [CrossRef]
31. Pavlov, M.; Siegbahn, P.E.M.; Sandström, M. Hydration of Beryllium, Magnesium, Calcium, and Zinc Ions Using Density Functional Theory. *J. Phys. Chem. A* **1998**, *102*, 219–228. [CrossRef]
32. De, S.; Ali, S.M.; Ali, A.; Gaikar, V.G. Micro-solvation of the Zn^{2+} ion—A case study. *Phys. Chem. Chem. Phys.* **2009**, *11*, 8285–8294. [CrossRef] [PubMed]
33. Cooper, T.E.; O'Brien, J.T.; Williams, E.R.; Armentrout, P.B. Zn^{2+} Has a Primary Hydration Sphere of Five: IR Action Spectroscopy and Theoretical Studies of Hydrated Zn^{2+} Complexes in the Gas Phase. *J. Phys. Chem. A* **2010**, *114*, 12646–12655. [CrossRef]
34. Obst, S.; Bradaczek, H. Molecular Dynamics Simulations of Zinc Ions in Water Using CHARMM. *J. Mol. Model.* **1997**, *3*, 224–232. [CrossRef]
35. Chillemi, G.; D'Angelo, P.; Pavel, N.V.; Sanna, N.; Barone, V. Development and Validation of an Integrated Computational Approach for the Study of Ionic Species in Solution by Means of Effective Two-Body Potentials. The Case of Zn^{2+}, Ni^{2+}, and Co^{2+} in Aqueous Solutions. *J. Am. Chem. Soc.* **2002**, *124*, 1968–1976. [CrossRef]
36. Arab, M.; Bougeard, D.; Smirnov, K.S. Molecular dynamics study of the structure and dynamics of Zn^{2+} ion in water. *Chem. Phys. Lett.* **2003**, *379*, 268–276. [CrossRef]
37. Inada, Y.; Mohammed, A.M.; Loeffler, H.H.; Funahashi, S. Water-Exchange Mechanism for Zinc(II), Cadmium(II), and Mercury(II) Ions in Water as Studied by Umbrella-Sampling Molecular-Dynamics Simulations. *Helv. Chim. Acta* **2005**, *88*, 461–469. [CrossRef]
38. Wu, J.C.; Piquemal, J.P.; Chaudret, R.; Reinhardt, P.; Ren, P. Polarizable Molecular Dynamics Simulation of Zn(II) in Water Using the AMOEBA Force Field. *J. Chem. Theory Comput.* **2010**, *6*, 2059–2070. [CrossRef]
39. Yu, H.; Whitfield, T.W.; Harder, E.; Lamoureux, G.; Vorobyov, I.; Anisimov, V.M.; MacKerell, A.D.; Roux, B. Simulating Monovalent and Divalent Ions in Aqueous Solution Using a Drude Polarizable Force Field. *J. Chem. Theory Comput.* **2010**, *6*, 774–786. [CrossRef]
40. Jana, C.; Ohanessian, G.; Clavaguéra, C. Theoretical insight into the coordination number of hydrated Zn^{2+} from gas phase to solution. *Theor. Chem. Acc.* **2016**, *135*, 141. [CrossRef]
41. Xu, M.; Zhu, T.; Zhang, J.Z.H. Molecular Dynamics Simulation of Zinc Ion in Water with an ab Initio Based Neural Network Potential. *J. Phys. Chem. A* **2019**, *123*, 6587–6595. [CrossRef] [PubMed]
42. Mohammed, A.M.; Loeffler, H.H.; Inada, Y.; Tanada, K.; Funahashi, S. Quantum mechanical/molecular mechanical molecular dynamic simulation of zinc(II) ion in water. *J. Mol. Liquids* **2005**, *119*, 55–62. [CrossRef]
43. Fatmi, M.Q.; Hofer, T.S.; Randolf, B.R.; Rode, B.M. An extended *ab initio* QM/MM MD approach to structure and dynamics of Zn(II) in aqueous solution. *J. Chem. Phys.* **2005**, *123*, 054514. [CrossRef] [PubMed]
44. Brancato, G.; Rega, N.; Barone, V. Microsolvation of the Zn(II) ion in aqueous solution: A hybrid QM/MM MD approach using non-periodic boundary conditions. *Chem. Phys. Lett.* **2008**, *451*, 53–57. [CrossRef]
45. Rega, N.; Brancato, G.; Petrone, A.; Caruso, P.; Barone, V. Vibrational analysis of x-ray absorption fine structure thermal factors by ab initio molecular dynamics: The Zn(II) ion in aqueous solution as a case study. *J. Chem. Phys.* **2011**, *134*, 074504. [CrossRef]
46. Riahi, S.; Roux, B.; Rowley, C.N. QM/MM Molecular Dynamics Simulations of the Hydration of Mg(II) and Zn(II) Ions. *J. Chem. Phys.* **2013**, *99*, 1–9. [CrossRef]
47. Fujiwara, T.; Mochizuki, Y.; Komeiji, Y.; Okiyama, Y.; Mori, H.; Nakano, T.; Miyoshi, E. Fragment molecular orbital-based molecular dynamics (FMO-MD) simulations on hydrated Zn(II) ion. *Chem. Phys. Lett.* **2010**, *490*, 41–45. [CrossRef]
48. Cauët, E.; Bogatko, S.; Weare, J.H.; Fulton, J.L.; Schenter, G.K.; Bylaska, E.J. Structure and dynamics of the hydration shells of the Zn^{2+} ion from ab initio molecular dynamics and combined ab initio and classical molecular dynamics simulations. *J. Chem. Phys.* **2010**, *132*, 194502. [CrossRef]
49. Liu, X.; Lu, X.; Wang, R.; Meijer, E.J. Understanding hydration of Zn^{2+} in hydrothermal fluids with ab initio molecular dynamics. *Phys. Chem. Chem. Phys.* **2011**, *13*, 13305–13309. [CrossRef]
50. Ducher, M.; Pietrucci, F.; Balan, E.; Ferlat, G.; Paulatto, L.; Blanchard, M. van der Waals Contribution to the Relative Stability of Aqueous Zn(2+) Coordination States. *J. Chem. Theory Comput.* **2017**, *13*, 3340–3347. [CrossRef]
51. Marx, D.; Hutter, J. *Ab Initio Molecular Dynamics*; Cambridge University Press: Cambridge, UK, 2009.
52. Hassanali, A.A.; Cuny, J.; Verdolino, V.; Parrinello, M. Aqueous solutions: State of the art in ab initio molecular dynamics. *Phil. Trans. R. Soc. A* **2014**, *372*, 20120482. [CrossRef] [PubMed]
53. Marx, D.; Sprik, M.; Parrinello, M. Ab initio molecular dynamics of ion solvation. The case of Be^{2+} in water. *Chem. Phys. Lett.* **1997**, *273*, 360–366. [CrossRef]
54. Śmiechowski, M.; Forbert, H.; Marx, D. Spatial decomposition and assignment of infrared spectra of simple ions in water from mid-infrared to THz frequencies: Li^+(aq) and F^-(aq). *J. Chem. Phys.* **2013**, *139*, 014506. [CrossRef] [PubMed]
55. Śmiechowski, M.; Sun, J.; Forbert, H.; Marx, D. Solvation shell resolved THz spectra of simple aqua ions – distinct distance- and frequency-dependent contributions of solvation shells. *Phys. Chem. Chem. Phys.* **2015**, *17*, 8323–8329. [CrossRef]

56. Chaudhari, M.I.; Soniat, M.; Rempe, S.B. Octa-Coordination and the Aqueous Ba^{2+} Ion. *J. Phys. Chem. B* **2015**, *119*, 8746–8753. [CrossRef]
57. Schienbein, P.; Schwaab, G.; Forbert, H.; Havenith, M.; Marx, D. Correlations in the Solute–Solvent Dynamics Reach Beyond the First Hydration Shell of Ions. *J. Phys. Chem. Lett.* **2017**, *8*, 2373–2380. [CrossRef]
58. Giacobello, F.; Mollica-Nardo, V.; Foti, C.; Ponterio, R.C.; Saija, F.; Trusso, S.; Sponer, J.; Cassone, G.; Giuffrè, O. Hydrolysis of Al^{3+} in Aqueous Solutions: Experiments and Ab Initio Simulations. *Liquids* **2022**, *2*, 26–38. [CrossRef]
59. Gregory, K.P.; Elliott, G.R.; Wanless, E.J.; Webber, G.B.; Page, A.J. A quantum chemical molecular dynamics repository of solvated ions. *Sci. Data* **2022**, *9*, 430. [CrossRef]
60. Śmiechowski, M. Unusual Influence of Fluorinated Anions on the Stretching Vibrations of Liquid Water. *J. Phys. Chem. B* **2018**, *122*, 3141–3152. [CrossRef]
61. Helm, L.; Merbach, A.E. Water exchange on metal ions: Experiments and simulations. *Coord. Chem. Rev.* **1999**, *187*, 151–181. [CrossRef]
62. Rotzinger, F.P. Treatment of Substitution and Rearrangement Mechanisms of Transition Metal Complexes with Quantum Chemical Methods. *Chem. Rev.* **2005**, *105*, 2003–2037. [CrossRef] [PubMed]
63. Kell, G.S. Density, Thermal Expansivity, and Compressibility of Liquid Water from 0 °C to 150 °C: Correlations and Tables for Atmospheric Pressure and Saturation Reviewed and Expressed on 1968 Temperature Scale. *J. Chem. Eng. Data* **1975**, *20*, 97–105. [CrossRef]
64. Pan, P.; Tremaine, P.R. Thermodynamics of aqueous zinc: Standard partial molar heat capacities and volumes of Zn^{2+}(aq) from 10 to 55 °C. *Geochim. Cosmochim. Acta* **1994**, *58*, 4867–4874. [CrossRef]
65. Marcus, Y. The Standard Partial Molar Volumes of Ions in Solution. Part 4. Ionic Volumes in Water at 0–100 °C. *J. Phys. Chem. B* **2009**, *113*, 10285–10291. [CrossRef] [PubMed]
66. Abraham, M.J.; Murtola, T.; Schulz, R.; Páll, S.; Smith, J.C.; Hess, B.; Lindahl, E. GROMACS: High performance molecular simulations through multi-level parallelism from laptops to supercomputers. *SoftwareX* **2015**, *1–22*, 19–25. [CrossRef]
67. Śmiechowski, M. Anion–water interactions of weakly hydrated anions: Molecular dynamics simulations of aqueous $NaBF_4$ and $NaPF_6$. *Mol. Phys.* **2016**, *114*, 1831–1846. [CrossRef]
68. Lagardère, L.; Jolly, L.H.; Lipparini, F.; Aviat, F.; Stamm, B.; Jing, Z.F.; Harger, M.; Torabifard, H.; Cisneros, G.A.; Schnieders, M.J.; et al. Tinker-HP: A massively parallel molecular dynamics package for multiscale simulations of large complex systems with advanced point dipole polarizable force fields. *Chem. Sci.* **2018**, *9*, 956–972. [CrossRef]
69. Laury, M.L.; Wang, L.P.; Pande, V.S.; Head-Gordon, T.; Ponder, J.W. Revised Parameters for the AMOEBA Polarizable Atomic Multipole Water Model. *J. Phys. Chem. B* **2015**, *119*, 9423–9437. [CrossRef]
70. The cp2k Developers Group. cp2k v. 6.0, 2001–2018. Available online: http://www.cp2k.org/ (accessed on 13 September 2022).
71. Hutter, J.; Iannuzzi, M.; Schiffmann, F.; VandeVondele, J. cp2k: Atomistic simulations of condensed matter systems. *WIREs Comput. Mol. Sci.* **2014**, *4*, 15–25. [CrossRef]
72. Kühne, T.D.; Iannuzzi, M.; Ben, M.D.; Rybkin, V.V.; Seewald, P.; Stein, F.; Laino, T.; Khaliullin, R.Z.; Schütt, O.; Schiffmann, F.; et al. CP2K: An electronic structure and molecular dynamics software package—Quickstep: Efficient and accurate electronic structure calculations. *J. Chem. Phys.* **2020**, *152*, 194103. [CrossRef]
73. VandeVondele, J.; Krack, M.; Mohamed, F.; Parrinello, M.; Chassaing, T.; Hutter, J. Quickstep: Fast and accurate density functional calculations using a mixed Gaussian and plane waves approach. *Comp. Phys. Commun.* **2005**, *167*, 103–128. [CrossRef]
74. Zhang, Y.; Yang, W. Comment on "Generalized Gradient Approximation Made Simple". *Phys. Rev. Lett.* **1998**, *80*, 890. [CrossRef]
75. Perdew, J.P.; Burke, K.; Ernzerhof, M. Generalized Gradient Approximation Made Simple. *Phys. Rev. Lett.* **1996**, *77*, 3865–3868. [CrossRef] [PubMed]
76. Marques, M.A.L.; Oliveira, M.J.T.; Burnus, T. Libxc: A library of exchange and correlation functionals for density functional theory. *Comp. Phys. Commun.* **2012**, *183*, 2272–2281. [CrossRef]
77. Marsalek, O.; Markland, T.E. Quantum Dynamics and Spectroscopy of Ab Initio Liquid Water: The Interplay of Nuclear and Electronic Quantum Effects. *J. Phys. Chem. Lett.* **2017**, *8*, 1545–1551. [CrossRef] [PubMed]
78. Duignan, T.T.; Baer, M.D.; Schenter, G.K.; Mundy, C.J. Real single ion solvation free energies with quantum mechanical simulation. *Chem. Sci.* **2017**, *8*, 6131–6140. [CrossRef] [PubMed]
79. Macchieraldo, R.; Esser, L.; Elfgen, R.; Voepel, P.; Zahn, S.; Smarsly, B.M.; Kirchner, B. Hydrophilic Ionic Liquid Mixtures of Weakly and Strongly Coordinating Anions with and without Water. *ACS Omega* **2018**, *3*, 8567–8582. [CrossRef] [PubMed]
80. Ohto, T.; Dodia, M.; Imoto, S.; Nagata, Y. Structure and Dynamics of Water at the Water–Air Interface Using First-Principles Molecular Dynamics Simulations within Generalized Gradient Approximation. *J. Chem. Theory Comput.* **2019**, *15*, 595–602. [CrossRef] [PubMed]
81. Ohto, T.; Dodia, M.; Xu, J.; Imoto, S.; Tang, F.; Zysk, F.; Kühne, T.D.; Shigeta, Y.; Bonn, M.; Wu, X.; et al. Accessing the Accuracy of Density Functional Theory through Structure and Dynamics of the Water–Air Interface. *J. Chem. Theory Comput.* **2019**, *10*, 4914–4919. [CrossRef]
82. Lippert, G.; Hutter, J.; Parrinello, M. A hybrid Gaussian and plane wave density functional scheme. *Mol. Phys.* **1997**, *92*, 477–487. [CrossRef]
83. VandeVondele, J.; Hutter, J. Gaussian basis sets for accurate calculations on molecular systems in gas and condensed phases. *J. Chem. Phys.* **2007**, *127*, 114105. [CrossRef] [PubMed]

84. Galib, M.; Duignan, T.T.; Misteli, Y.; Baer, M.D.; Schenter, G.K.; Hutter, J.; Mundy, C.J. Mass density fluctuations in quantum and classical descriptions of liquid water. *J. Chem. Phys.* **2017**, *146*, 244501. [CrossRef] [PubMed]
85. Goedecker, S.; Teter, M.; Hutter, J. Separable dual-space Gaussian pseudopotentials. *Phys. Rev. B* **1996**, *54*, 1703–1710. [CrossRef] [PubMed]
86. Jonchiere, R.; Seitsonen, A.P.; Ferlat, G.; Saitta, A.M.; Vuilleumier, R. Van der Waals effects in *ab initio* water at ambient and supercritical conditions. *J. Chem. Phys.* **2011**, *135*, 154503. [CrossRef]
87. Grimme, S.; Antony, J.; Ehrlich, S.; Krieg, H. A consistent and accurate *ab initio* parametrization of density functional dispersion correction (DFT-D) for the 94 elements H-Pu. *J. Chem. Phys.* **2010**, *132*, 154104. [CrossRef] [PubMed]
88. Durrant, T.R.; Murphy, S.T.; Watkins, M.B.; Shluger, A.L. Relation between image charge and potential alignment corrections for charged defects in periodic boundary conditions. *J. Chem. Phys.* **2018**, *149*, 024103. [CrossRef]
89. Bussi, G.; Donadio, D.; Parrinello, M. Canonical sampling through velocity rescaling. *J. Chem. Phys.* **2007**, *126*, 014101. [CrossRef]
90. Marzari, N.; Vanderbilt, D. Maximally localized generalized Wannier functions for composite energy bands. *Phys. Rev. B* **1997**, *56*, 12847–12865. [CrossRef]
91. Humphrey, W.; Dalke, A.; Schulten, K. VMD: Visual Molecular Dynamics. *J. Mol. Graph.* **1996**, *14*, 33–38. [CrossRef]
92. Racine, J. gnuplot 4.0: A portable interactive plotting utility. *J. Appl. Econom.* **2006**, *21*, 133–141. [CrossRef]
93. Brancato, G.; Barone, V. Free Energy Landscapes of Ion Coordination in Aqueous Solution. *J. Phys. Chem. B* **2011**, *115*, 12875–12878. [CrossRef] [PubMed]
94. Cooper, T.E.; Carl, D.R.; Armentrout, P.B. Hydration Energies of Zinc(II): Threshold Collision-Induced Dissociation Experiments and Theoretical Studies. *J. Phys. Chem. A* **2009**, *113*, 13727–13741. [CrossRef] [PubMed]
95. Marcus, Y. Ionic Radii in Aqueous Solutions. *Chem. Rev.* **1988**, *88*, 1475–1498. [CrossRef]
96. Pestana, L.R.; Mardirossian, N.; Head-Gordon, M.; Head-Gordon, T. Ab initio molecular dynamics simulations of liquid water using high quality meta-GGA functionals. *Chem. Sci.* **2017**, *8*, 3554–3565. [CrossRef]
97. Pestana, L.R.; Marsalek, O.; Markland, T.E.; Head-Gordon, T. The Quest for Accurate Liquid Water Properties from First Principles. *J. Phys. Chem. Lett.* **2018**, *9*, 5009–5016. [CrossRef]
98. Atta-Fynn, R.; Bylaska, E.J.; de Jong, W.A. Free energies and mechanisms of water exchange around Uranyl from first principles molecular dynamics. *Mater. Res. Soc. Symp. Proc.* **2012**, *1383*, 113–118. [CrossRef]